# Probing the determinants of the transglycosylation/hydrolysis partition in a retaining $\alpha$-l-arabinofuranosidase

Jiao Zhao, Tobias Tandrup, Bastien Bissaro, Sophie Barbe, Jens-Christian Poulsen, Isabelle André, Claire Dumon, Leila Lo Leggio, Michael O'Donohue, Régis Fauré

# Journal Pre-proof

Probing the determinants of the transglycosylation/hydrolysis partition in a retaining α-L-arabinofuranosidase

Jiao Zhao, Tobias Tandrup, Bastien Bissaro, Sophie Barbe, Jens-Christian N. Poulsen, Isabelle André, Claire Dumon, Leila Lo Leggio, Michael J. O'Donohue, Régis Fauré

Please cite this article as: Zhao J, Tandrup T, Bissaro B, Barbe S, Poulsen J-ChristianN, André I, Dumon C, Lo Leggio L, O'Donohue MJ, Fauré R, Probing the determinants of the transglycosylation/hydrolysis partition in a retaining α-<ce:small-caps>l</ce:small-caps>-arabinofuranosidase, *New BIOTECHNOLOGY* (2021), doi: https://doi.org/10.1016/j.nbt.2021.01.008

This is a PDF file of an article that has undergone enhancements after acceptance, such as the addition of a cover page and metadata, and formatting for readability, but it is not yet the definitive version of record. This version will undergo additional copyediting, typesetting and review before it is published in its final form, but we are providing this version to give early visibility of the article. Please note that, during the production process, errors may be discovered which could affect the content, and all legal disclaimers that apply to the journal pertain.

# Probing the determinants of the transglycosylation/hydrolysis partition in a retaining α-L-arabinofuranosidase

Jiao Zhao[a], Tobias Tandrup[b], Bastien Bissaro[a], Sophie Barbe[a], Jens-Christian N. Poulsen[b], Isabelle André[a], Claire Dumon[a], Leila Lo Leggio[b], Michael J. O'Donohue[a,*], Régis Fauré[a,*]

[a] *TBI, Université de Toulouse, CNRS, INRAE, INSA, Toulouse, France*

[b] *Department of Chemistry, University of Copenhagen, Copenhagen, Denmark*

[*] Corresponding authors.

*E-mail addresses:* michael.odonohue@inrae.fr (M.J. O'Donohue), regis.faure@insa-toulouse.fr (R. Fauré).

Graphical Abstract



## Highlights

- L352M alters donor and acceptor subsites, causing a domino effect in the active site.
- R69 is confirmed as a key determinant of the transglycosylation/hydrolysis partition.
- Active site flexibility contributes to the transglycosylation/hydrolysis equilibrium.
- N216W leads to a hydrophobic platform for better acceptor binding.
- A complex interplay of mutational effects procures better transglycosylase activity.

## ABSTRACT

The use of retaining glycoside hydrolases as synthetic tools for glycochemistry is highly topical and the focus of considerable research. However, due to the incomplete identification of the

molecular determinants of the transglycosylation/hydrolysis partition (T/H), rational engineering of retaining glycoside hydrolases to create transglycosylases remains challenging. Therefore, to understand better the factors that underpin transglycosylation in a GH51 retaining α-L-arabinofuranosidase from *Thermobacillus xylanilyticus,* the investigation of this enzyme's active site was pursued. Specifically, the properties of two mutants, F26L and L352M, located in the vicinity of the active site are described, using kinetic and 3D structural analyses and molecular dynamics simulations. The results reveal that the presence of L352M in the context of a triple mutant (also containing R69H and N216W) generates changes both in the donor and acceptor subsites, the latter being the result of a domino-like effect. Overall, the mutant R69H-N216W-L352M displays excellent transglycosylation activity (70% yield, 78% transfer rate and reduced secondary hydrolysis of the product). In the course of this study, the central role played by the conserved R69 residue was also reaffirmed. The mutation R69H affects both the catalytic nucleophile and the acid/base, including their flexibility, and has a determinant effect on the T/H partition. Finally, the results reveal that increased loop flexibility in the acceptor subsites creates new interactions with the acceptor, in particular with a hydrophobic binding platform composed of N216W, W248 and W302.

*Keywords:* biocatalysis; glycoside hydrolase; engineered transglycosylases; carbohydrate synthesis; molecular interactions; flexibility

*Database:* Structural data are available in the PDB database under the accession numbers 6ZT6 (R69H-L352M), 6ZT7 (R69H-L352M:A$^2$XX), 6ZT8 (R69H-N216W-L352M), 6ZT9 (R69H-N216W-L352M:A$^2$XX) and 6ZTA (R69H-G179F-L352M).

*Abbreviations:* L-Ara*f*, L-arabinofuranosyl unit; AXOS, arabinoxylo-oligosaccharides; A$^2$XX, α-L-Ara*f*-(1,2)-β-D-Xyl*p*-(1,4)-β-D-Xyl*p*-(1,4)-D-Xyl; A$^3$XX, α-L-Ara*f*-(1,3)-β-D-Xyl*p*-(1,4)-β-D-Xyl*p*-(1,4)-D-Xyl; DP, degree of polymerization; α-L-Ara*f*O*p*NP, 4-nitrophenyl α-L-arabinofuranoside; GT, glycosyltransferase; MD, molecular dynamics; *p*NP, 4-nitrophenol; rGH, retaining glycoside hydrolase; R$_T$, transfer rate; *Tx*Abf, α-L-arabinofuranosidase from *Thermobacillus xylanilyticus*; T/H, transglycosylation/hydrolysis ratio; TG, non-Leloir transglycosylase; TS, transition state; vdW, van der Waals; XOS, xylo-oligosaccharides; D-Xyl*p*, D-xylopyranosyl unit; X, D-xylose; X$_2$, (1,4)-β-D-xylobiose; X$_3$, (1,4)-β-D-xylotriose; X$_4$, (1,4)-β-D-xylotetraose; X$_5$, (1,4)-β-D-xylopentaose; X$_6$, (1,4)-β-D-xylohexaose; XA$^3$X, β-D-

Xyl$p$-(1,4)-[α-L-Ara$f$-(1,3)]-β-D-Xyl$p$-(1,4)-D-Xyl;  XA$^3$XX,  β-D-Xyl$p$-(1,4)-[α-L-Ara$f$-(1,3)]-β-D-Xyl$p$-(1,4)-β-D-Xyl$p$-(1,4)-D-Xyl.

3

## Introduction

The development of efficient *in vitro* strategies to synthesize carbohydrates remains a major challenge for synthetic chemistry. Despite considerable progress, the complexity and diversity of carbohydrates means that the quest for generic approaches remains highly topical and relevant for understanding their role in biological systems [1,2]. For decades, enzymes have been recognized as useful tools to tackle the complexity of carbohydrate chemistry and surmount the lack of selectivity of chemical catalysts. Among enzyme candidates, Leloir and non-Leloir carbohydrate-active enzymes are widely studied for their ability to synthesize various target glycoconjugates [3–5].

Leloir glycosyltransferases (GTs), which use sugar nucleotides as donors, can be considered as Nature's solution for carbohydrate synthesis, since *in vivo* these enzymes are responsible for the synthesis of most carbohydrates. However, harnessing GTs for the purposes of synthetic chemistry is fraught with challenges (e.g. expression of GTs in heterologous systems, the cost of sugar nucleotides, etc.) [6–8]. Therefore, despite recent progress in the area [9–11], the development of alternative strategies employing other enzyme classes, particularly retaining glycoside hydrolases (hereafter designated rGHs), is the subject of intense research. rGHs operate through a two-step displacement mechanism (**Figure 1**) [12] that provides the basis for the occurrence of non-Leloir transglycosylases (TGs), which are actually variants of rGHs that perform synthetic roles in biological systems [13,14]. Therefore, accounting for the facts that TGs naturally exist within the GH enzyme class and that rGHs are extremely abundant (at least 66% of all 888,506 classified GH modules among 83 of the 161 GH families in the CAZY database, http://www.cazy.org/ [15], January 2021) and cover a wide range of substrate specificities, makes this group of carbohydrate-active enzymes extremely interesting targets for synthetic chemists [16].

In the two-step mechanism used by rGHs, a covalent glycosyl-enzyme intermediate is formed that can either be deglycosylated by a water molecule (i.e. hydrolysis) or by a carbohydrate acceptor, which leads to transglycosylation [12,17]. In most rGHs operating in aqueous medium, hydrolysis is the principal outcome of the reaction, because of omnipresent water. However, naturally-occurring TGs reveal that specific protein modifications can diminish water-mediated deglycosylation and thus favour transglycosylation [16,18,19]. This evidence has prompted the creation of glycosynthetic rGHs using protein engineering, one of the best examples being the

4

glycosynthase strategy [20–23]. In this strategy, catalytically-impotent mutants are fed with fluoride-activated substrates. However, despite the relative simplicity of this elegant strategy, it is rather difficult to apply when using furanoside donors, because the synthesis of activated furanosyl fluorides has so far proven impossible. Alternative methods to engineer artificial TGs rely on the induction of shifts in the transglycosylation/hydrolysis (T/H) partition. This can be achieved either by engineering the reaction conditions (e.g. reducing water activity), or by modifying specific amino acids that influence the T/H partition [18,24,25].

Three main approaches have been identified to create TGs starting from rGHs [16]. The first involves the modification of substrate interactions in the donor subsite(s), leading to increased transition state (TS) energy barriers [26,27]. The aim is to reduce the efficiency of water-mediated deglycosylation, thus favouring transglycosylation, although overall catalytic activity is also affected. The second approach relies on modification of acceptor subsites (i.e. positively numbered subsites), the objective being to improve enzyme-acceptor interactions and thus favour sugar-mediated deglycosylation (i.e. transglycosylation). This is often achieved by introducing hydrophobic amino acid side chains at the acceptor site(s), which form favourable interactions with incoming glycoside acceptors and repel water molecules [26,28,29]. When combined with donor subsite engineering, the introduction of favourable acceptor site interactions can partially compensate for the overall reduction in efficiency due to the poor formation of the glycosyl-enzyme intermediate [30]. However, when acceptor subsite(s) engineering is used as a standalone strategy, it rarely affords radical diminution of hydrolysis [17]. The third method to modulate the T/H partition targets the ability of the enzyme to fix, convey and/or activate catalytic water molecules [31–34]. This generally requires knowledge related to the location of water channels and/or the identification of specific amino acids responsible for positioning water for catalysis.

Recent reports describe a semi-rational method to engineer TGs that involves targeting highly conserved residues that are located within, or in the vicinity of subsite -1 [27,35]. Interestingly, this approach is described as a potentially generic strategy [36]. However, despite this prospect and the previous use of a variety of techniques, including *in vitro* mutagenesis and *in silico* design (e.g. based on molecular dynamics (MD) simulations [34,37] and quantum mechanical/molecular mechanical studies [38,39]), an accurate and reliable method to predictably optimize the T/H partition has yet to be found.

5

In recent work performed on the GH51 α-L-arabinofuranosidase from *Thermobacillus xylanyliticus* (*Tx*Abf), a combinatory approach was used to create the first non-Leloir transarabinofuranosylases [17]. These enzymes are actually derivatives of *Tx*Abf bearing three mutations, R69H-N216W-L352M and R69H-G179F-L352M (**Figure 2**), which display remarkable transglycosylation capability (almost quantitative overall yield, with $A^2XX$ as main product that contains L-arabinofuranosyl (L-Ara*f*) unit linked to *O*-2 position of non-reducing end D-xylopyranosyl (D-Xyl*p*) unit of xylotriose, Figure 1; see [41] for a comprehensive description of arabinoxylo-oligosaccharides (AXOS) nomenclature) [17]. Each of the point mutations in these enzymes plays a distinct role in defining novel activity (Suppl. Table S1). In subsite -1, R69 lies within a H-bond distance (2.9 Å) of the catalytic nucleophile E298. It has been postulated that the mutation R69H impairs the nucleophilic strength of E298, leading to destabilization of $pK_a$ cycling, an intrinsic feature of the double-displacement mechanism [42]. N216W introduces hydrophobicity into subsite +2 and influences the positioning of the acceptor, thus increasing transglycosylation and regioselectivity for $A^2XX$. Additionally, forming part of subsite -1, L352M is located close (3.4 Å) to *O*-5 of the L-Ara*f* moiety. This mutation decreases the catalytic efficiency of *Tx*Abf [17]. Furthermore, an earlier study identified the mutation G179F that confers better xylotriose binding (Figure 2) [17]. Finally, in previous work F26L was pinpointed as a potential target to improve transglycosylation [43] and more recently this mutation was shown to confer increased ability to transfer the L-Ara*f* glycone of the donor onto a xylotriose acceptor [36]. Significantly, F26 is also located in subsite -1, is 3.8 Å distant from E298 and lies in the vicinity (3.8 Å) of the *O*-5 position of the L-Ara*f* moiety.

In the present study, a novel triple mutant F26L-R69H-N216W was constructed, providing the basis to compare this mutant with R69H-N216W-L352M, and thus appraise the relative impacts of F26L and L352M on the *Tx*Abf T/H partition. Moreover, two quadruple mutants were designed, F26L-R69H-N216W-L352M and R69H-G179F-N216W-L352M, to investigate the extent to which synergistic effects can be generated. To acquire atomic level insight, crystal structures of the mutated enzymes were solved and MD simulations performed.

## Materials and Methods

*Substrates and Chemicals*

The 4-nitrophenyl α-L-arabinofuranoside (α-L-Ara*f*O*p*NP) substrate was from Carbosynth Ltd. (Compton, UK; cat. no. 6892-58-6) and xylotriose from Wako Chemicals Europe GmbH

(Neuss, Germany; cat. no. 249-00651) respectively. The other xylo-oligosaccharides ($X_2$, O-XBI; $X_4$, O-XTE; $X_5$, O-XPE; $X_6$, O-XHE) were from Megazyme (Bray, Ireland; https://www.megazyme.com/shop-all-products/carbohydrates/oligosaccharides/1-4-beta-d-xylooligosaccharides). Molecular biology reagents were purchased from New England BioLabs (Evry, France).

*Mutagenesis, protein expression and purification*

*In vitro* site-directed mutagenesis was used to introduce single or multiple mutations within the *Tx*Abf (GenBank accession number CAA76421.2) contained in pET24-*Tx*Abf. Expression and purification of enzymes were performed as previously described [44,45]. Further details are provided in the Supplementary Material.

*Enzymatic assay*

Enzyme activities were measured using a previously described discontinuous assay [45]. To facilitate the comparison of data from different mutants, all reactions were operated at 45°C, as in previous work [17]. Specific activities (SA) of both hydrolysis ($SA_H$) and transglycosylation ($SA_T$) modes were measured by monitoring the release of 4-nitrophenol (*p*NP) from α-L-Ara*f*O*p*NP, as release of *p*NP relates to the common first step (glycosylation) in the double-displacement mechanism. Thus, herein SA values reflect global activity. This includes hydrolysis, self-condensation and (in the case of $SA_T$) transglycosylation onto XOS acceptors. All reactions were performed in triplicate at 45 °C using 5 mM α-L-Ara*f*O*p*NP as donor and, when relevant, 10 mM xylotriose as acceptor (i.e. with a constant [donor]/[acceptor] ratio of 2). Further experimental details are provided in the Supplementary Material.

Kinetic parameters and the efficiency coefficient $k_{cat}/K_M$ were determined by measuring enzyme SA at various substrate concentrations. While the reaction for wild-type was described by the classical Michaelis−Menten model (equation 1), the data in hydrolysis mode obtained for mutants were fitted to the modified Michaelis-Menten model (equation 2, which incorporates the nonspecific constant $N_S$ to account for self-condensation) using a nonlinear regression plot of SA versus [S] (substrate concentration).

$$SA = \frac{SA_{th}[S]}{K_M + [S]} \tag{1}$$

$$SA = \frac{SA_{th}[S]}{K_M + [S]} + Ns \cdot [S]$$

7

Concerning the two-substrate reaction of Ping-Pong Bi-Bi mechanism, the modified equation (3) was applied [17,46,47].

$$SA = \frac{SA_{th}[\text{Donor}] \cdot [\text{Acceptor}]}{K_M^{\text{Donor}}[\text{Acceptor}] + K_M^{\text{Acceptor}}[\text{Donor}] + [\text{Donor}] \cdot [\text{Acceptor}]} \qquad (3)$$

To capture information about transglycosylation reactions, donor- and acceptor-related kinetic parameters were measured by maintaining the acceptor (10 mM xylotriose) or donor (3 mM α-L-Ara$f$O$p$NP) constant while varying the other glycoside reactant. The two sets of data in transglycosylation mode were fitted to the Michaelis-Menten model represented by equation (1), thus yielding apparent $SA'_{th}$ and $K'_M$ or $SA''_{th}$ and $K''_M$. The parameters for donor and acceptor were then calculated from the derived equations (4) and (5) with $SA_{th}$ being the theoretical maximum activity achieved if the enzyme operates according to the Michaelis-Menten model. When fixing [Acceptor] at 10 mM and varying [Donor], the following is obtained:

$$SA'_{th} = \frac{[\text{Acceptor}]}{K_M^{\text{Acceptor}} + [\text{Acceptor}]} \cdot SA_{th} \qquad , \qquad K'_M = K_M^{\text{Donor}} \cdot \frac{[\text{Acceptor}]}{K_M^{\text{Acceptor}} + [\text{Acceptor}]} \qquad (4)$$

Similarly, when fixing [Donor] at 3 mM and varying [Acceptor], the following is obtained:

$$SA''_{th} = \frac{[\text{Donor}]}{K_M^{\text{Donor}} + [\text{Donor}]} \cdot SA_{th} \qquad , \qquad K''_M = K_M^{\text{Acceptor}} \cdot \frac{[\text{Donor}]}{K_M^{\text{Donor}} + [\text{Donor}]} \qquad (5)$$

*NMR analysis*

Reactions were performed at 45 °C in the presence of α-L-Ara$f$O$p$NP and xylotriose at a ratio of 1-2 (5 and 10 mM respectively) and enzyme in a total volume of 600 μL (containing 10% D$_2$O in 10 mM sodium phosphate buffer at pH 7.0 with 1 mg.mL$^{-1}$ bovine serum albumin (BSA, Sigma, Illkirch, France) in 5 mm NMR tubes. To initiate reactions, an aliquot of enzyme solution was added to the reaction, with different enzyme concentrations being applied to reach the maximal transglycosylation yield within a similar time delay (3 nM for *Tx*Abf, 0.13 μM for R69H-N216W, 0.22 μM for R69H-N216W-L352M, 0.60 μM for F26L-R69H-N216W, 1.79 μM for R69H-G179F-N216W-L352M and 0.57 μM for F26L-R69H-N216W-L352M). Details of NMR monitoring are described in the Supplementary Material.

Donor (α-L-Ara$f$O$p$NP) consumption and the appearance of AXOS as transglycosylation products were quantified by integrating the relevant anomeric proton signals from the internal anomeric proton from α-L-Ara$f$ unit (5.78 ppm for donor and shown in Tables for products), and normalized by the initial integral of α-L-Ara$f$O$p$NP. The AXOS yields (in %) were determined by product concentration against initial donor concentration. The transfer rate ($R_T$)

8

of the donor substrate onto xylotriose acceptor (μmol of formed $A^2XX$/μmol of consumed α-L-Ara$f$O$p$NP) was derived from the plot of $A^2XX$ transglycosylation yield as a function of donor conversion. Conveniently, being independent of the duration of the reaction, $R_T$ indicates the transglycosylation proportion in the consumed donor and allows to compare different enzymes that display both transglycosylation and hydrolysis.

*Crystallographic structure determination*

Crystals of *Tx*Abf mutants R69H-L352M, R69H-N216W-L352M and R69H-G179F-L352M were obtained at room temperature using the sitting-drop vapor diffusion method. For crystallization conditions, see Supplementary Material. To form crystallographic complex structures, soaking experiments were performed with crystals of mutants R69H-L352M and R69H-N216W-L352M by adding 2-5 µL of mother-liquor containing 33 to 330 mM of either $A^2XX$ or xylobiose.

Synchrotron diffraction data (Suppl. Table S2) were processed and scaled using either MOSFLM and AIMLESS [48,49], or XDS and XSCALE [50], all in the hexagonal space group $P6_522$. Refinement was performed in Refmac5 [51] of the CCP4 suite [52] alternated with manual building in COOT [53], with an initial rigid body refinement, using the structure and transferred $R_{Free}$ data of the E176Q:XA$^3$XX structure (PDB ID: 2VRQ), without substrate or solvent molecules.

*Molecular modelling procedures*

Starting from the high resolution crystal structures of *Tx*Abf (PDB ID: 2VRQ, including the above mentioned modifications) [40] and the mutant R69H-N216W-L352M (PDB ID: 6ZT8), 3D models were constructed for *Tx*Abf, R69H-N216W-L352M and F26L-R69H-N216W enzymes in complex with $A^2XX$. Missing residues 86-107 of the β2α2 loop in structures of mutants were added by comparison with the crystallographic structure of the wild-type enzyme (PDB ID: 2VRQ). Mutations not observed in X-ray structures were added using Pymol Molecular Graphics System (Schrödinger, Portland, OR, USA) [54]. $A^2XX$ was constructed using the *tleap* program in the AMBER software package and manually docked in the enzyme active site using as template co-crystallized E176Q:XA$^3$XX *Tx*Abf structure (PDB ID 2VRQ). In this conformation, the L-Ara$f$ moiety was placed in subsite -1 while D-Xyl$p$ units were positioned in +2', +1, +2 subsites. MD simulations were subsequently performed with the

9

AMBER ff14SB force-field [55] for enzymes and GLYCAM_06j [56] for carbohydrate ligands. Details of the MD protocol and analysis are described in the Supplementary Material. Graphics were prepared using Pymol Molecular Graphics System [54].

## Results

*Specific activity of wild-type* Tx*Abf and its mutants*

Assaying the specific activity of mutants in both hydrolysis ($SA_H$) and transglycosylation ($SA_T$) modes (i.e. in the absence or the presence of glycoside acceptor respectively; **Table 1**) revealed that all mutants displayed decreased $SA_H$ (0.1 to 40% compared to *Tx*Abf). However, unlike glycosynthases [57], catalytic activity remained measurable and significant in both modes. It is noteworthy that some mutants displayed a $SA_T/SA_H$ ratio >1, meaning that they preferentially performed transglycosylation in the presence of the acceptor. However, this enhanced capability correlated with decreased specific activity in both hydrolysis and transglycosylation modes (between 0.3 and 5.9% for $SA_T$ compared to the wild-type).

*Kinetic parameters in both hydrolytic and transglycosylation modes*

Kinetic parameters were determined in both hydrolysis and transglycosylation modes for donor and acceptor substrates individually. The kinetic profile of reactions catalysed by *Tx*Abf followed the classic Michaelis-Menten model (Equation 1), while mutants catalysing high levels of self-condensation in hydrolysis mode described a two-phase reaction trajectory that did not reach saturation, represented by a linear plot (**Figure 3**A). This result recalls the behaviour of *Tx*Abf R69-containing mutants and also that of *Thermus thermophilus* β-glycosidase consuming an *o*-nitrophenyl β-D-galactopyranoside donor, which also displayed a two-phase reaction profile [17,58]. To model this reaction, driven by an activated donor bearing a good leaving group ($pK_a$ of *p*NP = 7.18), a modified Michaelis-Menten equation (2) was used that contains a nonspecific constant ($N_S$). This constant reflects activation by the donor substrate, which drives self-condensation. Unlike hydrolysis mode, plotting SA as a function of either donor or acceptor concentration in transglycosylation mode generated curves that can be fitted using the Michaelis-Menten model for all enzymes. Nevertheless, even in the presence of 100 mM xylotriose, reactions catalysed by mutants failed to reach maximal rate, implying that saturation was not attained (Figure 3B). For *Tx*Abf and mutants R69H, L352M and R69H-L352M, a previous Brønsted-Hammett analysis has shown that when the donor substrate bears a good leaving group, such as *p*NP, deglycosylation constitutes the rate limiting step [17].

Accordingly, it is postulated that this is also true for the mutants N216W and G179F, since neither is sufficiently close to the donor binding site to impact on the nucleophile and/or acid/base residues. This assumption is also made for R69H-N216W-L352M and R69H-G179F-N216W-L352M, meaning that when the reaction involves a $p$NP-bearing donor the ratio $k_{cat}/K_M$ and the rate constant $k_{cat}$ correlate with the glycosylation and deglycosylation steps, respectively.

When operating in hydrolysis mode (**Table 2**), the three mutants displayed reduced (by nearly 1,000-fold) catalytic turnover compared to $Tx$Abf, which reflects impaired water-mediated deglycosylation. Consequently, since both glycosylation and deglycosylation TS display similar properties, it appears that glycosylation is also impacted, a claim that is supported by much lower $k_{cat}/K_M$ values compared to that of $Tx$Abf, these being in the range 0.2-1.9% of the wild-type value. Significantly, lowered catalytic efficiency has been previously described as an intrinsic feature of TGs [27,59]. Fortunately, in the case of F26L-R69H-N216W and R69H-G179F-N216W-L352M acting on α-L-Ara$f$O$p$NP, lower catalytic turnover is offset by lowered $K_M$ values, meaning that the glycosyl-enzyme intermediate is formed and displays a sufficiently long half-life to allow glycoside acceptor-mediated deglycosylation.

In transglycosylation mode (i.e., involving acceptor-mediated deglycosylation), equation (3) was used to fit the kinetic profiles of reactions catalysed by mutant enzymes. When using a constant concentration of 10 mM xylotriose acceptor (Table 2), the $k_{cat}$ value of the triple mutants increased 13- to 32-fold compared to the $k_{cat}$ value measured in hydrolysis mode. In addition, the presence of 10 mM acceptor barely altered (2-fold higher) the $K_M$ (donor) value of the reaction catalysed by R69H-N216W-L352M, but significantly increased that of F26L-R69H-N216W. Regarding the $k_{cat}/K_M$, the addition of 10 mM xylotriose led to a 6-fold increase in the reaction catalysed by R69H-N216W-L352M, but had little effect (17% decrease) on that containing F26L-R69H-N216W (Table 2). The fact that the $K_M$ (acceptor) value of the reaction involving F26L-R69H-N216W is 75 mM (**Table 3**) implies that the interaction of xylotriose with the enzyme is weak and probably explains why even at 10 mM it does not further increase catalytic efficiency.

*Transglycosylation profiles of mutants*
$H_2O$ to $D_2O$ exchange did not affect overall catalytic efficiency, nor the transglycosylation profiles of $Tx$Abf and mutants thereof (Suppl. Figure S1). Moreover, the kinetic parameters

11

(Tables 2-3 and Suppl. S3-S4) and transglycosylation yields (Suppl. Table S5) of reactions catalysed by R69H-L352M-N216W and F26L-R69H-N216W were only slightly sensitive to pH. However, transglycosylation yields were highly influenced by the acceptor/donor substrate ratio, with maximum yields being obtained at a ratio of 3.33 (Suppl. Table S6). On the other hand, for a given acceptor/donor substrate ratio, the global substrate concentrations (donor + acceptor) slightly affected yield (Suppl. Table S7). Taking all of these results into account the reaction conditions for time course ^{1}H NMR monitoring were defined [17].

When transferring α-L-Ara$f$ units onto xylotriose, $Tx$Abf produces a mixture of AXOS regioisomers at an overall 9% yield (Suppl. Figure S2), containing A[2]XX (4% yield, Table 4). All mutants bearing the substitution N216W displayed significantly improved regioselectivity, which drove the reaction towards the formation of A[2]XX, the yields of XA[3]X (β-D-Xyl$p$-(1,4)-[α-L-Ara$f$-(1,3)]-β-D-Xyl$p$-(1,4)-D-Xyl) and A[3]XX (α-L-Ara$f$-(1,3)-β-D-Xyl$p$-(1,4)-β-D-Xyl$p$-(1,4)-D-Xyl) being significantly reduced (Suppl. Figure S2) [17]. Since the distinctive anomeric signals of XA[3]X and A[3]XX (at 5.32 and 5.25 ppm respectively) are barely detectable during reactions catalysed by N216W-containing mutants, A[2]XX yield was used as an indicator of global transglycosylation efficiency. It is noteworthy that R69H-N216W-L352M maintains its regioselectivity towards the transfer of α-L-Ara$f$ moiety onto the $O$-2 position of the non-reducing end of XOS (Table S8).

Compared to $Tx$Abf, all mutants strongly modulated the T/H partition in favour of transglycosylation by combining both high transglycosylation yields (57-70%) and high $R_T$ (59-78%, Suppl. Table S9), with R69H being the principal cause of these enhancements [17]. Nevertheless, other amino acid substitutions provided contributions that led to more subtle improvements. The previously generated R69H-N216W-L352M proved to be the most potent enzyme (up to 70% yield and $R_T$ of 78%) for A[2]XX synthesis (**Figure 4** and Suppl. Table S9). Even though the transglycosylation yield of F26L-R69H-N216W was close to that of R69H-N216W (Table 4), F26L promoted higher $R_T$ (1.1-fold) and alleviated secondary hydrolysis when combined with R69H-N216W (Suppl. Table S9). Adding F26L to the most potent triple mutant background (i.e., F26L + R69H-N216W-L352M) slightly lowered A[2]XX synthesis, while maintaining the self-condensation level (12%). In this respect, while all mutants synthesized A[2]XX as the major transglycosylation product, mutants R69H-N216W and F26L-R69H-N216W displayed increased self-condensation capability (17-20% yield) and the introduction of L352M mutation to any of the mutants restored self-condensation to an

intermediate level (11-12% yield). This is indicative of enhanced competition between xylotriose (acceptor) and α-L-Ara$f$OpNP (both donor and acceptor) for occupation of the positive subsites. The addition of G179F to R69H-N216W-L352M was intended to reduce secondary hydrolysis of A$^2$XX. However, in addition to significant diminution of secondary hydrolysis (Table S9), this mutation actually led to 24% reduction in A$^2$XX yield (**Table 4** and Figure 4).

Secondary hydrolysis was exhibited when the linearity of donor concentration-dependent A$^2$XX production was lost (Figure 4B), the linearity tipping point being best observed when A$^2$XX yield/donor consumption (in %) is plotted against donor consumption (Suppl. Figure S3). For R69H-G179F-N216W-L352M, despite displaying a lower R$_T$, the tipping point occurred when the donor was almost completely (97%) consumed. However, for the mutants R69H-N216W-L352M, F26L-R69H-N216W and F26L-R69H-N216W-L352M, it was observed earlier at a mean value of 82% (Suppl. Table S9).

*Transglycosylation using XOS*

To evaluate the impact of degree of polymerization (DP) of the acceptor on the ability of R69H-N216W-L352M to perform transglycosylation, D-xylose (X, DP = 1) and a range of XOS, from xylobiose to xylohexaose, were used in reactions containing α-L-Ara$f$O$p$NP. When using X as the acceptor, transglycosylation was barely detectable, with the yield being 2 and 5% respectively for the two regioisomer products (undetermined linkages). The use of longer XOS (DP ≥ 2) as acceptor procured products that were all detected at 5.20 ppm (at 45 °C) meaning that each of the AXOS products shared the same regioselectivity (i.e. the α-L-Ara$f$ moiety was linked to the *O*-2 position of the non-reducing end of the XOS) as the product generated when xylotriose was used as acceptor [60–62]. Moreover, the use of XOS displaying a DP ≥ 2 generated transglycosylation products at high yield (63-75%) and secondary hydrolysis was almost identical (Suppl. Figure S4), although SA$_T$ decreased as a function of increasing acceptor DP (Suppl. Table S8).

*3D structure of mutants R69H-L352M and R69H-N216W-L352M*

The crystal structures of *apo*-R69H-L352M and *apo*-R69H-N216W-L352M revealed that L352M provokes a domino-like effect in its neighbouring environment. In particular, both W302 and W248, which were previously reported to interact with both the donor at subsite -1

(W302) and acceptor within subsites +1 and +2 (both residues) [40], are displaced by L352M (**Figure 5**A and C). Despite the fact that a structure bearing F26L is not available, it was postulated that this mutation will have a much shorter range effect, affecting only subsite -1. Indeed, this is supported by the observation that the L352M (combined with R69H-N216W) mutation has greater influence on the T/H ratio in favour of transglycosylation.

Considering R69H, structural analysis shows that the shorter histidine side chain induces a conformational change of N175 (Figure 5B-C). In both the seleno-methionine substituted wild-type structure and that of the mutant E176Q (PDB ID: 2VRK and 2VRQ respectively), residue N175 interacts with both the acid/base (E176) and the nucleophile (E298). As mentioned, the R69 residue is within H-bond distance (2.9 Å) of the nucleophile. This distance is increased to 6.0 Å in the R69H mutant. Therefore, R69H has a significant effect, both directly and indirectly, on the catalytic apparatus.

In regard to the N216W mutation, the data clearly indicate that the presence of tryptophan in subsite +2 provides a productive substrate interaction that probably reinforces acceptor binding. Analysis of structures of R69H-L352M and R69H-N216W-L352M derived from crystals soaked in $A^2XX$ failed to reveal any substrate-induced alterations. However, it is important to note that both enzymes are active and thus *in situ* cleavage of $A^2XX$ is unavoidable. Furthermore, MPD from the crystallization conditions may interfere with the binding of the substrate. Consequently, only the L-Ara*f* subunit was detected in the active site, present in two conformations (Suppl. Figure S5).

Unfortunately, the dataset of the mutant containing G179F displayed lower resolution and was thus more difficult to exploit. Nevertheless, the presence of phenylalanine at position 179 appears to create a new hydrophobic interaction platform (Suppl. Figure S6). However, the poor quality of the structure does not permit deeper analysis of putative structural rearrangements. Data collection and refinement statistics for all crystal structures are presented in Suppl. Table S2.

*Molecular dynamics simulations on* Tx*Abf and its mutants F26L-R69H-N216W and R69H-N216W-L352M in complex with $A^2XX$ product*

Analysis of the MD simulation performed on the *Tx*Abf:$A^2XX$ complex (i.e. with transglycosylation product) revealed that the oligosaccharide remained bound to the enzyme

14

throughout the 20 ns simulation. Binding of $A^2XX$ was stabilized by a network of van der Waals (vdW) interactions involving F26 and Y242 in subsite -1, H98 and W99 in subsite +2', and W248 and W302 in subsite +1 (**Figure 6**A). Generally, the loops surrounding the active site appear to be stabilized by the presence of the ligand, consistent with previous observations (Suppl. Figure S7) [63]. In comparison with wild-type enzyme, the MD simulation performed on F26L-R69H-N216W revealed only slight conformational differences in the vicinity of the active site. One notable exception concerns the apparently greater flexibility of the β4α4 loop that bears the catalytic acid/base E176 (Figure 6, S7 and S8). Regarding subsite +2, most of the ligand-binding features are conserved, the main difference being the introduction of a tryptophan residue at position 216. This provides an additional stacking interaction with D-Xyl*p* moieties. Consequently, this mutation confers the means on F26L-R69H-N216W to bind xylotriose in a distinct way, different from that of *Tx*Abf (Figure 6A-B).

Finally, MD simulation revealed that combining L352M with R69H-N216W led to greater conformational rearrangements of loops β6α6 and β7α7, compared to both *Tx*Abf and F26L-R69H-N216W (Suppl. Figure S8). On the other hand, the flexibility of loop β8α8, bearing the L352M, was identical in all the enzymes studied (Suppl. Figure S7). Together these dynamic behavioural differences increase the solvent exposure of the active site of R69H-N216W-L352M compared to *Tx*Abf [33]. Additionally, the introduction of a methionyl moiety at position 352 appears to provoke a domino cascade that affects the conformation of residues (particularly W302 and W248) in subsites +1 and +2 (Figure 6C), consistent with the results from crystallography. Interestingly, this diminishes vdW interactions between the xylotriosyl moiety of $A^2XX$ and W302 and W248, causing it to move away from loops β6α6 and β7α7. Compared to *Tx*Abf, these changes translate into a distinct binding mode involving a novel vdW interaction with the opposite face of the tryptophanyl moiety in position 216 (Figure 6C).

## Discussion

A previous study closely analysed the transglycosylation reaction performed by the retaining α-L-arabinofuranosidase, *Tx*Abf, and provided clues on how to further alter the T/H ratio in favour of transglycosylation [17]. Accordingly, the best performing mutant is the result of three point mutations, R69H, N216W, and L352M. In this work, the aim was to investigate further the impact of L352M as well as to compare its effect with that of another subsite -1 mutation, F26L.

15

*Two subsite -1 residues contribute differently to the active site*

Mutations F26L and L352M display different effects on the T/H ratio of *Tx*Abf, consistent with the fact that F26, a highly conserved residue in family GH51 [36], participates exclusively to subsite -1, whereas residue L352 (less conserved) [64] is located in a more ambiguous position between subsite -1 and the acceptor subsites. Both R69H-N216W-L352M and F26L-R69H-N216W demonstrate outstanding transglycosylation ability, coupled to low catalytic efficiency ($k_{cat}/K_M$). This latter observation supports the postulate that both naturally occurring and engineered TGs are generally less efficient catalysts than their hydrolytic counterparts [16,27,65]. This impaired catalytic ability is probably related to more energy-demanding TS for both glycosylation and deglycosylation steps (Suppl. Table S10) [16,17], and thus the prolonged lifetime of the covalent glycosyl-enzyme intermediate [66]. On the other hand, the extended lifetime of the glycosyl-enzyme intermediate is likely to favour statistically unfavourable deglycosylation by the glycoside acceptor (0.01 M), which is a minority species compared to water (55.6 M). In hydrolysis mode, F26L-R69H-N216W displayed a remarkable decrease in the values of both $K_M$ and $k_{cat}$, suggesting that F26L severely disturbs the ability of the pocket-like subsite -1 to bind the donor substrate in a productive configuration for water-mediated deglycosylation. In contrast, the results for R69H-N216W-L352M (relatively unchanged $K_M$ value and lower $k_{cat}$), clearly indicate that the impact of the L352M-bearing mutant mainly affects the deglycosylation step [17]. It is noteworthy that the use of xylotriose as acceptor further demonstrates the different effects engendered by F26L and L352M. Even though the $k_{cat}$ values are enhanced in the presence of xylotriose, the F26L-bearing enzyme appears less able to bind xylotriose (higher $K_M$ value for acceptor and lower $R_T$) than the L352M-bearing one, implying that the latter generates a positive effect with regard to xylotriose binding in acceptor subsites.

*The conserved residue R69 plays a key role in T/H modulation*

R69 is fully conserved throughout clan GH-A [67] and thus in GH51 [17,68]. Therefore, the fact that all R69H-N216W-derived mutants display similar transglycosylation profiles (including self-condensation) leads to the proposal that R69H is the driving force that tips T/H ratio in favour of transglycosylation. To muster support for this postulate, it is first relevant to note that in transglycosylation mode all R69H-containing mutants display activation in the presence of acceptor ($SA_T/SA_H > 1$, Table 1). Moreover, when comparing hydrolysis and

transglycosylation modes, the $k_{cat}$ values are significantly improved for the latter. This suggests that deglycosylation by glycoside acceptors is enhanced. Combined with the fact that R69H affects the p$K_a$ of both nucleophile and acid base [17], the structural analysis supports the claim that mutation of R69 to histidine indirectly affects one or both of the catalytic residues. In the case of the catalytic acid/base E176, it appears that this occurs by modifying the hydrogen bond network that involves the conserved residue N175 and indeed this is observed in the MD simulation (Figure 6B-C). This modification almost certainly affects the protonation capability of E176 and thus impairs the ability of the enzyme to activate incoming acceptors (irrespective of whether it is a water molecule or a glycoside acceptor). In turn, it can be postulated that this partially diminishes the thermodynamic advantage of water (although water concentration remains a determining factor), and concomitantly increases the likelihood of deglycosylation by glycoside acceptors (p$K_a$ of xylose = 12.15) [69], which display lower deprotonation enthalpy than water [70]. Finally, it is also relevant to note that N175 is thought to be involved in TS stabilization [39]. Therefore, the indirect modification of the interaction N175···OH-2 of α-L-Ara$f$ unit by R69H might increase the TS energy barriers (Table S10) [16,17].

*Active site flexibility modulates T/H*

The results of previous work performed on a TG/hydrolytic rGH pair from family GH16 (clan GH-B) has led to the proposal that alterations in local active site flexibility (i.e., plasticity and adaptation) can shift the T/H partition in favor of transglycosylation [71]. In this study, enhanced transglycosylation was attributed to increased flexibility in the donor subsite, coupled to more flexibility in the acceptor site. In contrast, the study of GH31 TG/rGH pair (clan GH-D) revealed that enhanced transglycosylation could be the result of conformational rigidity and the intervention of a 'hydrophobic shield' that prevents nucleophilic attack by catalytic water [19]. Finally, in a recent study increased transglycosylation was partly ascribed to higher local flexibility of the catalytic acid/base residue adding entropic cost to the height of the free energy barrier of the reaction, and thus slowing the hydrolysis step. Reciprocally, this favours (or increases the probability) of acceptor-mediated deglycosylation [72]. In the present work, comparison of the root-mean-square-fluctuations (RMSF, Suppl. Figure S7) along the protein sequence clearly reveal that the best performing TG R69H-N216W-L352M displays higher flexibility in acceptor subsites, particularly in loops β6α6 and β7α7, bearing W248 and W302 respectively (Suppl. Figure S8). Considering the enhancement of the affinity (lower $K_M$ value) for the acceptor, it can be suggested that this is due to greater flexibility. Additionally, R69H-

N216W-L352M and F26L-R69H-N216W, which display higher transfer rates than R69H-N216W (78% and 67% compared to 59% respectively), provides evidence that higher flexibility of the acid/base E176 might also enhance the T/H partition, which is consistent with the aforementioned findings [72].

*Acceptor subsite determinants*

The data reveal a significant difference in the ability of D-xylose and XOS to act as acceptors and show that XOS (DP > 2) are the best ones. These observations clearly point to the fact that the binding ability of the native subsite +1 alone is insufficient and that modifications, including the addition of a putative subsite +2, are essential for enhancement of transglycosylation. In this regard, the mutant R69H-N216W-L352M no doubt creates the conditions for better acceptor binding. Significantly, the presence of hydrophobic residues in positively numbered-binding sites has already been identified as a key determinant of TG activity in other GHs [73,74]. In the case of the GH35 β-galactosidases from *Aspergillus niger*, it was reported that F264, Y304, and W806 constitute a dynamic hydrophobic platform that accommodates the sugar at subsite +1. In the case of *Tx*Abf and its mutants, it is likely that the hydrophobicity of subsite +1 is insufficient, whereas molecular modelling of the R69H-N216W-L352M:$A^2XX$ complex indicates that both W216 and W248 are involved in stacking interactions with the subsite +2 D-Xyl*p* moiety. Finally, it is noteworthy that both the $SA_T$ and yield decrease for XOS with DP $\geq$ 3 (Suppl. Table S8), which implies that extra D-Xyl*p* moieties are less well-accommodated, although the presence of an undetected subsite +3 cannot be fully excluded.

*Synergistic effects of mutations affect secondary hydrolysis*

As a lone mutation, L352M eliminates secondary hydrolysis of $A^2XX$, and its combination with R69H does not alter this property [17]. However, to some extent the addition of N216W to R69H-L352M restores secondary hydrolysis, even though $A^2XX$ synthesis is enhanced. In the present study, it is confirmed that while the combination of L352M with R69H-N216W decreases (2-fold) the synthesis rate, it nevertheless improves $R_T$ (1.3-fold) and the $A^2XX$ synthesis/secondary hydrolysis ratio ($v_T/v_{HII}$, 1.4-fold; Table S9). The conclusion of these observations is that L352M alone creates this effect, impacting the conformational flexibility of the neighbouring W302 and W248 residues and, in turn, diminishing $A^2XX$ hydrolysis. However, this beneficial trait is probably partially countered by the effect of N216W, which apparently creates a hydrophobic platform (i.e., W302 + W248 + N216W, W178 also might be

18

involved) that provides the basis of productive positioning for xylotriose-mediated deglycosylation toward $A^2XX$ synthesis, followed by a distinct binding mode with an altered positioning less favourable for its hydrolysis.

It can be assumed that G179F binds α-L-Ara$f$O$p$NP more tightly thanks to the creation of a more hydrophobic environment (Suppl. Figure S6) and stronger interaction with the $p$NP moiety [17]. The kinetic data presented here support this assumption, because the catalytic efficiency of hydrolysis catalysed by R69H-G179F-N216W-L352M is significantly increased (5.3-fold) compared to that of R69H-N216W-L352M, this change being driven by a decrease of the $K_M$ value.It is likely that better donor binding by R69H-G179F-N216W-L352M leads to the acceleration of the glycosylation rate. Noticeably, even though transglycosylation yield, $R_T$ and $v_T$ are unfavourably affected by the introduction of G179F, secondary hydrolysis ($v_{HII}$) of the transglycosylation product is delayed and drastically reduced. This infers that binding of the $p$NP-bearing donor is more efficient than that of $A^2XX$, which only becomes significant once α-L-Ara$f$O$p$NP is almost depleted.

## Conclusions

In the present work, enzyme kinetics, 3D structure determination and molecular dynamics simulations have been combined to further elucidate the molecular determinants that promote T/H partition in *Tx*Abf mutants. The results provide further evidence supporting the postulate that R69H is a key T/H modulator. The introduction of histidine 69 disrupts the hydrogen bond network of both catalytic residues, thus leading to hydrolytic inactivity. In addition, it is shown that L352M plays a dual effect, affecting both subsite -1 and, through a domino-like effect, the acceptor subsites. The F26L-containing mutant is a less efficient TG than the prototype R69H-N216W-L352M, because its impact is limited to subsite -1. Overall, the results are consistent with the suggestion that glycosyl-transferring GHs are sluggish enzymes (lower $k_{cat}/K_M$ values) when compared to hydrolytic counterparts and that relaxed donor binding and acid/base flexibility can contribute to enhancement of transglycosylation. Finally, the results are consistent with the postulate that strengthened interactions with incoming glycoside acceptors contribute to T/H shifts in favor of transglycosylation. Together they further underline that finding a generic strategy to alter the T/H partition in rGHs is not simple (but neither impossible), because the switch from hydrolysis to transglycosylation is the result of a significant number of subtle modifications to the active site.

19

## Acknowledgments

## Funding

## Declaration of Competing Interest

None.

## Appendix A. Supplementary data

Supplementary material related to this article can be found, in the online version, at doi:.

# References

[1] Danby PM, Withers SG. Advances in enzymatic glycoside synthesis. ACS Chem Biol 2016;11:1784–94. https://doi.org/10.1021/acschembio.6b00340.

[2] Krasnova L, Wong CH. Oligosaccharide synthesis and translational innovation. J Am Chem Soc 2019;141:3735–54. https://doi.org/10.1021/jacs.8b11005.

[3] Trincone A, Giordano A. Glycosyl hydrolases and glycosyltransferases in the synthesis of oligosaccharides. Curr Org Chem 2006;10:1163–93. https://doi.org/10.2174/138527206777698075.

[4] Filice M, Marciello M. Enzymatic synthesis of oligosaccharides: a powerful tool for a sweet challenge. Curr Org Chem 2013;17:701–18. https://doi.org/10.2174/1385272811317070006.

[5] Benkoulouche M, Fauré R, Remaud-Siméon M, Moulis C, André I. Harnessing glycoenzyme engineering for synthesis of bioactive oligosaccharides. Interface Focus 2019;9:20180069. https://doi.org/10.1098/rsfs.2018.0069.

[6] Field RA. Challenging reaction equilibria. Nat Chem Biol 2011;7:658–9. https://doi.org/10.1038/nchembio.668.

[7] Chang A, Singh S, Phillips GN, Thorson JS. Glycosyltransferase structural biology and its role in the design of catalysts for glycosylation. Curr Opin Biotechnol 2011;22:800–8. https://doi.org/10.1016/j.copbio.2011.04.013.

[8] Nidetzky B, Gutmann A, Zhong C. Leloir glycosyltransferases as biocatalysts for chemical production. ACS Catal 2018;8:6283–300. https://doi.org/10.1021/acscatal.8b00710.

[9] Eisele A, Zaun H, Kuballa J, Elling L. In vitro one-pot enzymatic synthesis of hyaluronic acid from sucrose and *N*-acetylglucosamine: optimization of the enzyme module system and nucleotide sugar regeneration. ChemCatChem 2018;10:2969–81. https://doi.org/10.1002/cctc.201800370.

[10] Mestrom L, Przypis M, Kowalczykiewicz D, Pollender A, Kumpf A, Marsden SR, et al. Leloir glycosyltransferases in applied biocatalysis: a multidisciplinary approach. Int J Mol Sci 2019;20:5263. https://doi.org/10.3390/ijms20215263.

[11] Kallolimath S, Gruber C, Steinkellner H, Castilho A. Promoter choice impacts the efficiency of plant glyco-engineering. Biotechnol J 2018;13:1700380. https://doi.org/10.1002/biot.201700380.

[12] Koshland DE. Stereochemistry and the mechanism of enzymatic reactions. Biol Rev 1953;28:416–36. https://doi.org/10.1111/j.1469-185X.1953.tb01386.x.

[13] Baumann MJ, Eklöf JM, Michel G, Kallas ÅM, Teeri TT, Czjzek M, et al. Structural evidence for the Evolution of xyloglucanase activity from xyloglucan *endo*-transglycosylases: biological implications for cell wall metabolism. Plant Cell 2007;19:1947–63. https://doi.org/10.1105/tpc.107.051391.

[14] Passerini D, Vuillemin M, Ufarté L, Morel S, Loux V, Fontagné-Faucher C, et al. Inventory of the GH70 enzymes encoded by *Leuconostoc citreum* NRRL B-1299 - identification of three novel α-transglucosylases. FEBS J 2015;282:2115–30. https://doi.org/10.1111/febs.13261.

[15] Lombard V, Golaconda Ramulu H, Drula E, Coutinho PM, Henrissat B. The

carbohydrate-active enzymes database (CAZy) in 2013. Nucleic Acids Res 2014;42:D490–5. https://doi.org/10.1093/nar/gkt1178.

[16] Bissaro B, Monsan P, Fauré R, O'Donohue MJ. Glycosynthesis in a waterworld: new insight into the molecular basis of transglycosylation in retaining glycoside hydrolases. Biochem J 2015;467:17–35. https://doi.org/10.1042/BJ20141412.

[17] Bissaro B, Durand J, Planas A, Monsan P, Biarnés X, Planas A, et al. Molecular design of non-Leloir furanose-transferring enzymes from an α-L-arabinofuranosidase: a rationale for the engineering of evolved transglycosylases. ACS Catal 2015;5:4598–611. https://doi.org/10.1021/acscatal.5b00949.

[18] Abdul Manas NH, Md. Illias R, Mahadi NM. Strategy in manipulating transglycosylation activity of glycosyl hydrolase for oligosaccharide production. Crit Rev Biotechnol 2018;38:272–93. https://doi.org/10.1080/07388551.2017.1339664.

[19] Light SH, Cahoon LA, Mahasenan K V., Lee M, Boggess B, Halavaty AS, et al. Transferase versus hydrolase: the role of conformational Flexibility in Reaction Specificity. Structure 2017;25:295–304. https://doi.org/10.1016/j.str.2016.12.007.

[20] Moracci M, Trincone A, Perugino G, Ciaramella M, Rossi M. Restoration of the activity of active-site mutants of the hyperthermophilic β-glycosidase from *Sulfolobus solfataricus*: dependence of the mechanism on the action of external nucleophiles. Biochemistry 1998;37:17262–70. https://doi.org/10.1021/bi981855f.

[21] Malet C, Planas A. From β-glucanase to β-glucansynthase: glycosyl transfer to α-glycosyl fluorides catalyzed by a mutant endoglucanase lacking its catalytic nucleophile. FEBS Lett 1998;440:208–12. https://doi.org/10.1016/S0014-5793(98)01448-3.

[22] Mackenzie LF, Wang Q, Warren RAJ, Withers SG. Glycosynthases: Mutant glycosidases for oligosaccharide synthesis. J Am Chem Soc 1998;120:5583–4. https://doi.org/10.1021/ja980833d.

[23] Mayer C, Zechel DL, Reid SP, Warren RAJ, Withers SG. The E358S mutant of *Agrobacterium* sp. β-glucosidase is a greatly improved glycosynthase. FEBS Lett 2000;466:40–4. https://doi.org/10.1016/S0014-5793(99)01751-2.

[24] Huber RE, Gaunt MT, Sept RL, Babiak MJ. Differences in the effects of pH on the hydrolytic and transgalactosylic reactions of β-galactosidase (*Escherichia coli*). Can J Biochem Cell Biol 1983;61:198–206. https://doi.org/10.1139/o83-028.

[25] Wang LX, Huang W. Enzymatic transglycosylation for glycoconjugate synthesis. Curr Opin Chem Biol 2009;13:592–600. https://doi.org/10.1016/j.cbpa.2009.08.014.

[26] Madhuprakash J, Dalhus B, Rani TS, Podile AR, Eijsink VGH, Sørlie M. Key residues affecting transglycosylation activity in family 18 chitinases: insights into donor and acceptor subsites. Biochemistry 2018;57:4325–37. https://doi.org/10.1021/acs.biochem.8b00381.

[27] Teze D, Hendrickx J, Czjzek M, Ropartz D, Sanejouand Y-H, Tran V, et al. Semi-rational approach for converting a GH1 β-glycosidase into a β-transglycosidase. Prot Eng Des Sel 2014;27:13–9. https://doi.org/10.1093/protein/gzt057.

[28] Rivera MH, López-Munguía A, Soberón X, Saab-Rincón G. α-amylase from *Bacillus licheniformis* mutants near to the catalytic site: effects on hydrolytic and transglycosylation activity. Protein Eng 2003;16:505–14. https://doi.org/10.1093/protein/gzg060.

[29] Rosengren A, Reddy SK, Sjöberg JS, Aurelius O, Logan DT, Kolenová K, et al. An *Aspergillus nidulans* β-mannanase with high transglycosylation capacity revealed through comparative studies within glycosidase family 5. Appl Microbiol Biotechnol 2014;98:10091–104. https://doi.org/10.1007/s00253-014-5871-8.

[30] Zakariassen H, Hansen MC, Jøranli M, Eijsink VGH, Sørlie M. Mutational effects on transglycosylating activity of family 18 chitinases and construction of a hypertransglycosylating mutant. Biochemistry 2011;50:5693–703. https://doi.org/10.1021/bi2002532.

[31] Kuriki T, Kaneko H, Yanase M, Takata H, Shimada J, Handa S, et al. Controlling substrate preference and transglycosylation activity of neopullulanase by manipulating steric constraint and hydrophobicity in active center. J Biol Chem 1996;271:17321–9.

[32] Teze D, Hendrickx J, Dion M, Tellier C, Woods VL, Tran V, et al. conserved water molecules in family 1 glycosidases: a DXMS and molecular dynamics study. Biochemistry 2013;52:5900–10. https://doi.org/10.1021/bi400260b.

[33] David B, Irague R, Jouanneau D, Daligault F, Czjzek M, Sanejouand Y-H, et al. Internal water dynamics control the transglycosylation/hydrolysis balance in the agarase (AgaD) of *Zobellia galactanivorans*. ACS Catal 2017;7:3357–67. https://doi.org/10.1021/acscatal.7b00348.

[34] Florindo RN, Souza VP, Mutti HS, Camilo C, Manzine LR, Marana SR, et al. Structural insights into β-glucosidase transglycosylation based on biochemical, structural and computational analysis of two GH1 enzymes from *Trichoderma harzianum*. N Biotechnol 2018;40:218–27. https://doi.org/10.1016/j.nbt.2017.08.012.

[35] Teze D, Daligault F, Ferrières V, Sanejouand YH, Tellier C. Semi-rational approach for converting a GH36 α-glycosidase into an α-transglycosidase. Glycobiology 2015;25:420–7. https://doi.org/10.1093/glycob/cwu124.

[36] Teze D, Zhao J, Wiemann M, Kazi ZG, Lupo R, Rønne ME, et al. Rational enzyme design without structural knowledge: a sequence-based approach for efficient generation of glycosylation catalysts. ChemRxiv 2020. Preprint. https://doi.org/10.26434/chemrxiv.11538708.v2.

[37] Jamek SB, Muschiol J, Holck J, Zeuner B, Busk PK, Mikkelsen JD, et al. Loop protein engineering for improved transglycosylation activity of a β-*N*-acetylhexosaminidase. ChemBioChem 2018;19:1858–65. https://doi.org/10.1002/cbic.201800181.

[38] Romero-Téllez S, Lluch JM, González-Lafont À, Masgrau L. Comparing hydrolysis and transglycosylation reactions catalyzed by *Thermus thermophilus* β-glycosidase. A combined MD and QM/MM study. Front Chem 2019;7:200. https://doi.org/10.3389/fchem.2019.00200.

[39] Raich L, Borodkin V, Fang W, Castro-López J, van Aalten DMF, Hurtado-Guerrero R, et al. A trapped covalent intermediate of a glycoside hydrolase on the pathway to transglycosylation. Insights from experiments and quantum mechanics/molecular mechanics simulations. J Am Chem Soc 2016;138:3325–32. https://doi.org/10.1021/jacs.5b10092.

[40] Paës G, Skov LK, O'Donohue MJ, Rémond C, Kastrup JS, Gajhede M, et al. The structure of the complex between a branched pentasaccharide and *Thermobacillus xylanilyticus* GH-51 arabinofuranosidase reveals xylan-binding determinants and induced fit. Biochemistry 2008;47:7441–51. https://doi.org/10.1021/bi800424e.

[41] Fauré R, Courtin CM, Delcour JA, Dumon C, Faulds CB, Fincher GB, et al. A brief and informationally rich naming system for oligosaccharide motifs of heteroxylans found in plant cell walls. Aust J Chem 2009;62:533–7. https://doi.org/10.1071/CH08458.

[42] McIntosh LP, Hand G, Johnson PE, Joshi MD, Körner M, Plesniak LA, et al. The p$K_a$ of the general acid/base carboxyl group of a glycosidase cycles during catalysis: a ^{13}C-NMR study of *Bacillus circulans* xylanase. Biochemistry 1996;35:9958–66. https://doi.org/10.1021/bi9613234.

[43] Arab-Jaziri F, Bissaro B, Dion M, Saurel O, Harrison D, Ferreira F, et al. Engineering transglycosidase activity into a GH51 α-L-arabinofuranosidase. N Biotechnol 2013;30:536–44. https://doi.org/10.1016/j.nbt.2013.04.002.

[44] Debeche T, Cummings N, Connerton I, Debeire P, O'Donohue MJ. Genetic and biochemical characterization of a highly thermostable α-L-arabinofuranosidase from *Thermobacillus xylanilyticus*. Appl Environ Microbiol 2000;66:1734–6. https://doi.org/10.1128/AEM.66.4.1734-1736.2000.

[45] Bissaro B, Saurel O, Arab-jaziri F, Saulnier L, Milon A, Tenkanen M, et al. Mutation of a pH-modulating residue in a GH51 α-L-arabinofuranosidase leads to a severe reduction of the secondary hydrolysis of transfuranosylation products. Biochim Biophys Acta, Gen Subj 2014;1840:626–36. https://doi.org/10.1016/j.bbagen.2013.10.013.

[46] Cleland WW. Enzyme kinetics. Annu Rev Biochem 1967;36:77–112. https://doi.org/10.1146/annurev.bi.36.070167.000453.

[47] Silva RG, Schramm VL. Uridine phosphorylase from *Trypanosoma cruzi*: kinetic and chemical mechanisms. Biochemistry 2011;50:9158-9166. https://doi.org/10.1021/bi2013382.

[48] Battye TGG, Kontogiannis L, Johnson O, Powell HR, Leslie AGW. iMOSFLM: a new graphical interface for diffraction-image processing with MOSFLM. Acta Crystallogr Sect D Biol Crystallogr 2011;67:271–81. https://doi.org/10.1107/S0907444910048675.

[49] Evans PR, Murshudov GN. How good are my data and what is the resolution? Acta Crystallogr Sect D Biol Crystallogr 2013;69:1204–14. https://doi.org/10.1107/S0907444913000061.

[50] Kabsch W. XDS. Acta Crystallogr Sect D Biol Crystallogr 2010;66:125–32. https://doi.org/10.1107/S0907444909047337.

[51] Murshudov GN, Vagin AA, Dodson EJ. Refinement of macromolecular structures by the maximum-likelihood method. Acta Crystallogr Sect D Biol Crystallogr 1997;53:240–55. https://doi.org/10.1107/S0907444996012255.

[52] Winn MD, Ballard CC, Cowtan KD, Dodson EJ, Emsley P, Evans PR, et al. Overview of the CCP4 suite and current developments. Acta Crystallogr Sect D Biol Crystallogr 2011;67:235–42. https://doi.org/10.1107/S0907444910045749.

[53] Emsley P, Cowtan K. Coot: model-building tools for molecular graphics. Acta Crystallogr Sect D Biol Crystallogr 2004;60:2126–32. https://doi.org/10.1107/S0907444904019158.

[54] DeLano W. The PyMOL Molecular Graphics System. Delano Scientific, San Carlos, CA. 2002.

[55] Maier JA, Martinez C, Kasavajhala K, Wickstrom L, Hauser KE, Simmerling C. ff14SB: improving the accuracy of protein side chain and backbone parameters from ff99SB. J

Chem Theory Comput 2015;11:3696–713. https://doi.org/10.1021/acs.jctc.5b00255.

[56] Kirschner KN, Yongye AB, Tschampel SM, González-Outeiriño J, Daniels CR, Foley BL, et al. GLYCAM06: a generalizable biomolecular force field. J Comput Chem 2008;29:622–55. https://doi.org/10.1002/jcc.20820.

[57] Perugino G, Trincone A, Rossi M, Moracci M. Oligosaccharide synthesis by glycosynthases. Trends Biotechnol 2004;22:31–7. https://doi.org/10.1016/j.tibtech.2003.10.008.

[58] Feng HY, Drone J, Hoffmann L, Tran V, Tellier C, Rabiller C, et al. Converting a β-glycosidase into a β-transglycosidase by directed evolution. J Biol Chem 2005;280:37088–97. https://doi.org/10.1074/jbc.M502873200.

[59] Durand J, Biarnés X, Watterlot L, Bonzom C, Borsenberger V, Planas A, et al. A single point mutation alters the transglycosylation/hydrolysis partition, significantly enhancing the synthetic capability of an *endo*-glycoceramidase. ACS Catal 2016;6:8264–75. https://doi.org/10.1021/acscatal.6b02159.

[60] Viëtor RJ, Hoffmann RA, Angelino SAGF, Voragen AGJ, Kamerling JP, Vliegenthart JFG. Structures of small oligomers liberated from barley arabinoxylans by endoxylanase from *Aspergillus awamori*. Carbohydr Res 1994;254:245–55.

[61] Pastell H, Tuomainen P, Virkki L, Tenkanen M. Step-wise enzymatic preparation and structural characterization of singly and doubly substituted arabinoxylo-oligosaccharides with non-reducing end terminal branches. Carbohydr Res 2008;343:3049–57. https://doi.org/10.1016/j.carres.2008.09.013.

[62] Ferré H, Broberg A, Duus J, Thomsen KK. A novel type of arabinoxylan arabinofuranohydrolase isolated from germinated barley. Analysis of substrate preference and specificity by nano-probe NMR. Eur J Biochem 2000;267:6633–41. https://doi.org/10.1046/j.1432-1327.2000.01758.x.

[63] Arab-Jaziri F, Bissaro B, Barbe S, Saurel O, Débat H, Dumon C, et al. Functional roles of H98 and W99 and β2α2 loop dynamics in the α-L-arabinofuranosidase from *Thermobacillus xylanilyticus*. FEBS J 2012;279:3598–611. https://doi.org/10.1111/j.1742-4658.2012.08720.x.

[64] Arab-Jaziri F, Bissaro B, Tellier C, Dion M, Fauré R, O'Donohue MJ. Enhancing the chemoenzymatic synthesis of arabinosylated xylo-oligosaccharides by GH51 α-L-arabinofuranosidase. Carbohydr Res 2015;401:64–72. https://doi.org/10.1016/j.carres.2014.10.029.

[65] Luang S, Cho J Il, Mahong B, Opassiri R, Akiyama T, Phasai K, et al. Rice Os9BGlu31 is a transglucosidase with the capacity to equilibrate phenylpropanoid, flavonoid, and phytohormone glycoconjugates. J Biol Chem 2013;288:10111–23. https://doi.org/10.1074/jbc.M112.423533.

[66] Piens K, Fauré R, Sundqvist G, Baumann MJ, Saura-Valls M, Teeri TT, et al. Mechanism-based labeling defines the free energy change for formation of the covalent glycosyl-enzyme intermediate in a xyloglucan *endo*-transglycosylase. J Biol Chem 2008;283:21864–72. https://doi.org/10.1074/jbc.M803057200.

[67] Zhang Y, Ju J, Peng H, Gao F, Zhou C, Zeng Y, et al. Biochemical and structural characterization of the intracellular mannanase AaManA of *Alicyclobacillus acidocaldarius* reveals a novel glycoside hydrolase family belonging to clan GH-A. J Biol Chem 2008;283:31551–8. https://doi.org/10.1074/jbc.M803409200.

[68]  Borsenberger V, Dornez E, Desrousseaux M-L, Massou S, Tenkanen M, Courtin CM, et al. A $^1$H NMR study of the specificity of α-L-arabinofuranosidases on natural and unnatural substrates. Biochim Biophys Acta, Gen Subj 2014;1840:3106–14. https://doi.org/10.1016/j.bbagen.2014.07.001.

[69]  In: Bhattacharyya L, Rohrer JS, editors. Applications of ion chromatography for pharmaceutical and biological products. 1st Edition. John Wiley & Sons, Inc.; 2012, p 455-456.

[70]  Geronimo I, Payne CM, Sandgren M. The role of catalytic residue p$K_a$ on the hydrolysis/transglycosylation partition in family 3 β-glucosidases. Org Biomol Chem 2018;16:316–24. https://doi.org/10.1039/c7ob02558k.

[71]  Mark P, Baumann MJ, Eklöf JM, Gullfot F, Michel G, Kallas ÅM, et al. Analysis of nasturtium *Tm*NXG1 complexes by crystallography and molecular dynamics provides detailed insight into substrate recognition by family GH16 xyloglucan *endo*-transglycosylases and *endo*-hydrolases. Proteins Struct Funct Bioinforma 2009;75:820–36. https://doi.org/10.1002/prot.22291.

[72]  David B, Arnaud P, Tellier C, Sanejouand Y-H. Toward the design of efficient transglycosidases: the case of the GH1 of *Thermus thermophilus*. Protein Eng Des Sel 2019;32:309–16. https://doi.org/10.1093/protein/gzz032.

[73]  Umemoto N, Ohnuma T, Osawa T, Numata T, Fukamizo T. Modulation of the transglycosylation activity of plant family GH18 chitinase by removing or introducing a tryptophan side chain. FEBS Lett 2015;589:2327–33. https://doi.org/10.1016/j.febslet.2015.07.018.

[74]  Rico-Díaz A, Ramírez-Escudero M, Vizoso-Vázquez Á, Cerdán ME, Becerra M, Sanz-Aparicio J. Structural features of *Aspergillus niger* β-galactosidase define its activity against glycoside linkages. FEBS J 2017;284:1815–29. https://doi.org/10.1111/febs.14083.

## Figures and Tables Legends

**Fig. 1.** Two-step displacement mechanism (also known as Ping-Pong Bi Bi mechanism in transglycosylation) of retaining *Tx*Abf. The first step (glycosylation) leads to release of the *p*NP leaving group from the donor, α-L-Ara*f*O*p*NP in this study, and concomitant formation of the covalent glycosyl-enzyme intermediate. Regarding the second step (deglycosylation), the covalent glycosyl-enzyme intermediate can be attacked by either a water molecule (hydrolysis) or an external acceptor (transglycosylation with xylotriose as acceptor in this study). In the case of secondary hydrolysis, the transglycosylation product becomes a donor substrate with a subsequent deglycosylation step involving water.
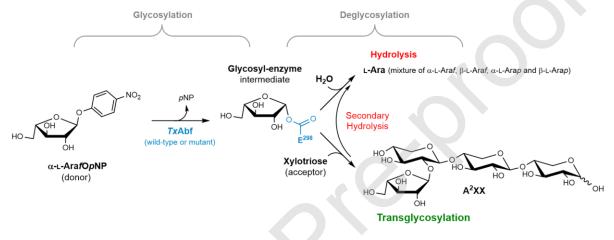


Figure 1.

**Fig. 2.** View of the *Tx*Abf-E176Q:XA³XX complex active site (PDB ID: 2VRQ) [40] showing the positioning of F26, R69, G179, N216 and L352 residues as well as the mutated acid/base (A/B) E176Q and the catalytic nucleophile (Nu) E298 (Table S1). The reducing D-Xyl*p* unit, X in black, of pentasaccharide XA³XX (i.e., β-D-Xyl*p*-(1,4)-[α-L-Ara*f*-(1,3)]-β-D-Xyl*p*-(1,4)-β-D-Xyl*p*-(1,4)-D-Xyl*p*) is not observed.
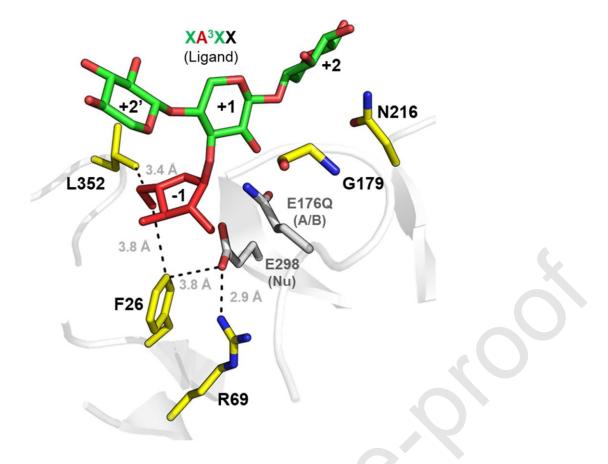
**Figure 2.**

**Fig. 3.** Steady-state kinetics of F26L-R69H-N216W and R69H-N216W-L352M. (A) F26L-R69H-N216W in hydrolysis (●) and transglycosylation (○) modes. (B) SA$_T$ as a function of xylotriose concentration indicating the acceptor-mediated activation of F26L-R69H-N216W (●) and R69H-N216W-L352M (○) in transglycosylation mode with fixed 3 mM α-L-Ara$f$O$p$NP as donor. Mutant F26L-R69H-N216W in hydrolysis mode displays a two-phase reaction that fits to a modified Michaelis-Menten model (equation 2), which accounts for activation by α-L-Ara$f$O$p$NP, while the other curves fit to equation 1 (i.e., the classical Michaelis-Menten model).
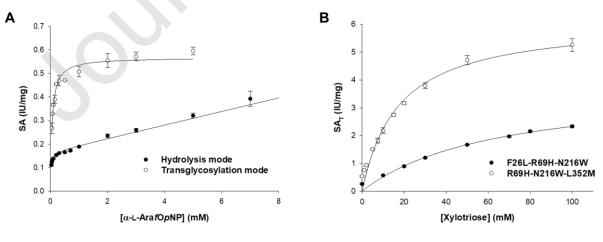


Figure 3.

28

**Fig. 4.** NMR monitoring of A$^2$XX evolution as a function of (A) time and (B) donor conversion. All assays were carried out at 45 °C and pH 7.0 in buffered 10% D$_2$O, with 5 mM α-L-Ara$f$O$p$NP and 10 mM xylotriose as donor and acceptor respectively.
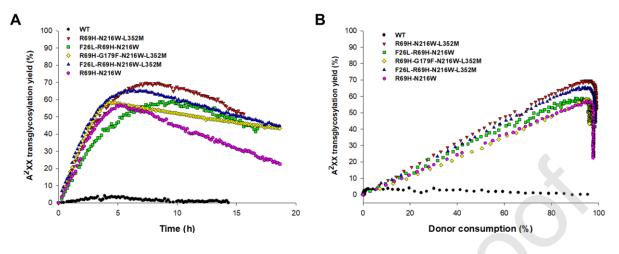


Figure 4.

**Fig. 5.** (A) and (B) Superposition of $Tx$Abf (in blue, PDB ID: 2VRQ, ligand XA$^3$XX omitted) and R69H-L352M (in orange, PDB ID: 6ZT6). 2F$_o$-F$_c$ electron density shown at 1.0 σ cut-off in orange mesh. H-bonds shown as black dashes with distances indicated). (C) Schematic representation of the primary and secondary effects of the mutations (Table S1). Mutations R69H, N216W and L352M analysed in this study (in green) are shown along with residues that are putatively affected by displaying altered electrostatic interactions (in blue) and those that are proposed to be involved in substrate binding (in red). The corresponding coloured dotted arrows either indicate the location of catalytic processes or the site of binding interactions. Open black arrows indicate secondary effects by changes in coordinates resulting from a mutation.
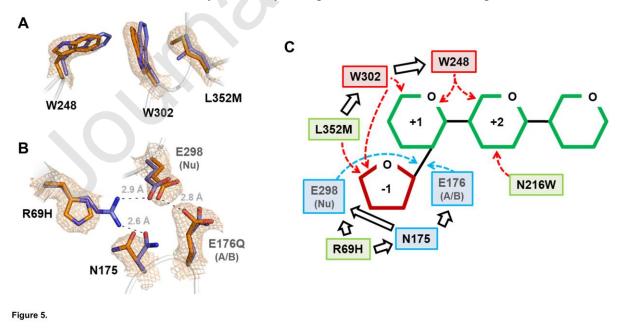


Figure 5.

**Fig. 6.** Active site view of distinct conformations observed along MD simulations of (A) *Tx*Abf, (B) mutant F26L-R69H-N216W and (C) mutant R69H-N216W-L352M. Catalytic residues are coloured in yellow. Selected amino acid residues are shown in stick format and coloured in graduated (from light to dark) blue tones that represent film stills of the MD simulation. $A^2XX$ is shown as sticks, coloured in magenta for L-Ara*f* and green for the xylotriosyl moiety, in the initial and final conformations. Mutated residues are highlighted by framed labels.
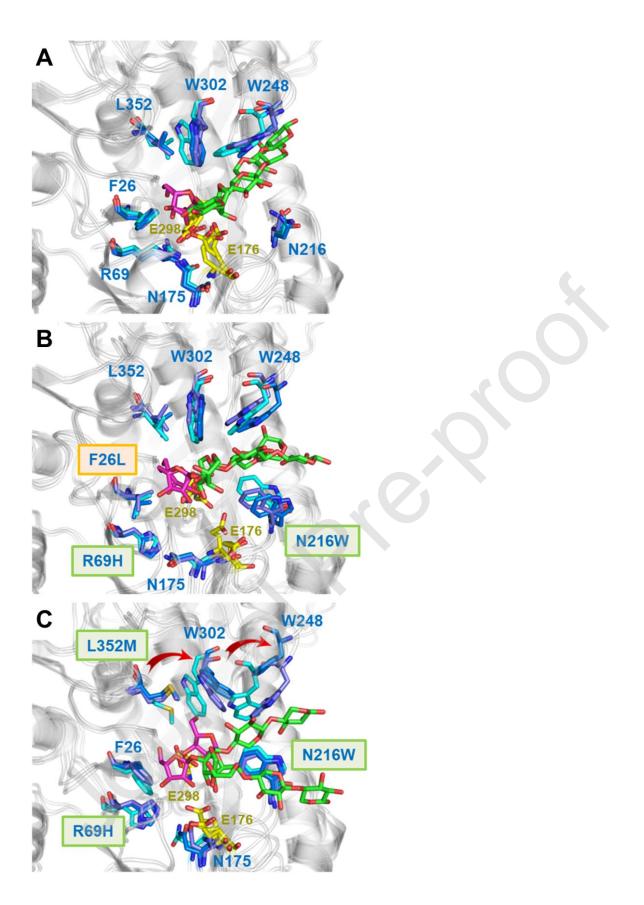
**Figure 6.**

**Table 1.** Specific activities in hydrolysis (SA$_H$) and transglycosylation (SA$_T$) modes.

**Table 2.** Kinetic parameters on α-L-Ara$f$O$p$NP (donor) in hydrolysis mode and transglycosylation mode at pH 7.0.

**Table 3.** Kinetic parameters on xylotriose (acceptor) in transglycosylation mode at pH 7.0.

**Table 4.** A$^2$XX transglycosylation and self-condensation yields (determined by NMR) for reactions catalysed by *Tx*Abf and mutants thereof.

**Table 1**

Specific activities in hydrolysis (SA$_H$) and transglycosylation (SA$_T$) modes.[1]

| Enzyme | SA$_H$[2] (IU.mg$^{-1}$) | SA$_T$[3] (IU.mg$^{-1}$) | SA$_T$/SA$_H$[4] |
|---|---|---|---|
| wt | 261.79 | 125.49 | 0.5 |
| F26L | 105.76 | 83.26 | 0.8 |
| R69H | 2.84 | 7.41 | 2.6 |
| L352M[5] | 86.91 | 47.00 | 0.5 |
| R69H-N216W | 1.60 | 2.89 | 1.8 |
| R69H-N216W-L352M | 0.97 | 1.82 | 1.9 |
| F26L-R69H-N216W | 0.32 | 0.60 | 1.9 |
| R69H-G179F-N216W-L352M | 0.29 | 0.42 | 1.4 |
| F26L-R69H-N216W-L352M | 0.27 | 0.93 | 3.4 |

[1]One unit (IU) of enzyme specific activity corresponds to the amount of enzyme releasing 1 μmol of $p$NP per minute. Experiments were performed in triplicate and standard deviations (S.D.) were always less than 10%.

[2]Reactions operating in hydrolysis mode contain only 5 mM α-L-Ara$f$O$p$NP.

[3]Reactions operating in transglycosylation mode contain both donor (5 mM α-L-Ara$f$O$p$NP) and acceptor (10 mM xylotriose).

[4]The ratio between SA$_T$ and SA$_H$ reveals the extent of activation or inhibition by the acceptor.

[5]SA of L352M was calculated using previously reported data acquired in the same reaction conditions (i.e., 45 °C in 50 mM sodium phosphate buffer at pH 7.0) [17].

**Table 2**

Kinetic parameters on α-L-Ara$f$O$p$NP (donor)[1] in hydrolysis mode and transglycosylation mode[2] (data shown in bracket) at pH 7.0.

| Enzyme | SA$_{th}$ (IU.mg$^{-1}$) | $K_M$ (mM) | $k_{cat}$ (s$^{-1}$) | $k_{cat}/K_M$ (s$^{-1}$.mM$^{-1}$) | N$_S$[3] (s$^{-1}$.mM$^{-1}$) |
|---|---|---|---|---|---|
| wt[4] | 145 | 0.25 | 139 | 556 | - |
| R69H-N216W-L352M[4] | 0.60 (7.76) | 0.48 (1.03) | 0.58 (7.46) | 1.21 (7.24) | 0.03 (-) |
| F26L-R69H-N216W | 0.16 (4.98) | 0.01 (0.53) | 0.15 (4.78) | 10.81 (9.02) | 0.03 (-) |
| R69H-G179F-N216W-L352M | 0.14 | 0.02 | 0.14 | 6.45 | 0.03 |

[1]Experiments were performed in triplicate and S.D. were always less than 10%.

[2]In transglycosylation mode, the concentration of xylotriose acceptor was fixed at 10 mM.

[3]N$_S$ is a nonspecific constant that is included in the modified Michaelis-Menten equation (2) to account for activation of the enzyme by the self-condensation product: SA$_{app}$ = SA$_{th}$·[S]/($K_M$ + [S]) + N$_S$·[S] where SA$_{th}$ is the theoretical maximum activity achieved if the enzyme operates according to the Michaelis-Menten model.

[4]Data in hydrolysis mode from previous work acquired in the same conditions [17].

**Table 3**

Kinetic parameters on xylotriose (acceptor) in transglycosylation mode at pH 7.0.[1]

| Enzyme | SA$_{max}$ (IU.mg$^{-1}$) | $K_M$ (mM) | $k_{cat}$ (s$^{-1}$) | $k_{cat}/K_M$ (s$^{-1}$.mM$^{-1}$) |
|---|---|---|---|---|
| R69H-N216W-L352M | 8.28 | 23.32 | 7.96 | 0.34 |
| F26L-R69H-N216W | 4.49 | 75.43 | 4.31 | 0.06 |

[1]The concentration of α-L-Ara$f$O$p$NP donor was fixed at 3 mM. Experiments were performed in triplicate and s.d. were always less than 10%.

**Table 4**

33

A$^2$XX transglycosylation and self-condensation yields (determined by NMR) for reactions catalysed by *Tx*Abf and mutants thereof.[1]

| Enzyme | Yield (%) | | |
|---|---|---|---|
| | A$^2$XX | Self-condensation (1,2)[2] | Self-condensation (1,3)[2] |
| | 5.20 ppm[3] | 5.88 ppm[3] | 5.81 ppm[3] |
| wt | 4 | 5 | 1 |
| R69H-N216W | 57 | 2 | 18 |
| R69H-N216W-L352M | 70 | 2 | 9 |
| F26L-R69H-N216W | 59 | 2 | 15 |
| R69H-G179F-N216W-L352M | 59 | 3 | 9 |
| F26L-R69H-N216W-L352M | 66 | 2 | 10 |

[1]Kinetic assays were carried out using 5 mM α-L-Ara*f*O*p*NP and 10 mM xylotriose at 45 °C and pH 7.0 in buffered 10% D$_2$O.

[2]Self-condensation products are α-L-Ara*f*-(1,2)-α-L-Ara*f*O*p*NP and α-L-Ara*f*-(1,3)-α-L-Ara*f*O*p*NP.

[3]NMR chemical shift of the anomeric proton of transferred α-L-Ara*f* unit of products at 45 °C.